

**Evolutionary, multi-scale analysis of river bank line retreat using  
continuous wavelet transforms: Jamuna River, Bangladesh.**

Mount, Nick J.<sup>1\*</sup>, Tate, Nicholas J.<sup>2</sup>, Sarker, Maminul H.<sup>3</sup> and Thorne, Colin R.<sup>1</sup>

\* Corr. Auth. nick.mount@nottingham.ac.uk, Tel: +44 (0)115 951 5438, Fax: +44 (0)115 951 15249

<sup>1</sup>. School of Geography, University of Nottingham, University Park, Nottingham, NG7 2RD, UK.

<sup>2</sup>. Department of Geography, University of Leicester, Leicester, LE1 7RH, UK.

<sup>3</sup>. Centre for Environmental and Geographic Information Services, House 6, Road 23/C, Gulshan-1, Dhaka 1212, Bangladesh.

## **Abstract**

In this study continuous wavelet transforms are used to explore spatio-temporal patterns of multi-scale bank line retreat along a 204 km reach of the Jamuna River, Bangladesh. A sequence of eight bank line retreat series, derived from remotely-sensed imagery for the period 1987-1999, is transformed using the Morlet mother wavelet. Bank erosion is shown to operate at several characteristic spatial and temporal scales. Local erosion and bank line retreat are shown to occur in short, well defined reaches characterised by temporal persistence at the same location, and separated by relatively stable reaches. In contrast, evidence of downstream propagation of bank line retreat patterns is evident at larger spatial scales. The intensity of localised bank line retreat (i.e. at scales of 0 - 20 km) is strongly related to the magnitude of monsoonal peak discharge, but this relationship weakens as the spatial scale of erosion increases. The potential of continuous wavelet analysis to enhancing our understanding of morphological evolution in complex fluvial systems with multi-channel planforms is discussed.

## **Keywords**

Continuous Wavelet Transform, Jamuna River, Braided river, Time-space, Erosion processes, Embayment pattern, Sediment wave.

## **1. Introduction**

The planform evolution of the Jamuna River, Bangladesh, the distal portion of the Brahmaputra, has been the focus of many studies in which the aim has been to assess, characterise and quantify the magnitude and distribution of bank line migration (e.g. Coleman, 1969; Sarma and Basumallick, 1984; Singh et al., 1990; Thorne et al., 1993, 1995; Thorne and Russell, 1993; Halcrow, 1994; Goswami, 1995; Goswami et al., 1999; Ashworth et al., 2000; CEGIS, 2000, 2007; Khan and Islam, 2003; Sarma and Phukan, 2004, 2006; Sankhua et al., 2005; Sarma, 2005; Takagi et al., 2007). However, quantification and prediction of the spatio-temporal patterns of bank line migration

exhibited by the river are complicated by its large geographical scale (here synonymous with extent) and its complex planform, which features elements of meandering, braiding and anastomosing (Fergusson, 1993). The large geographical scale has thus far precluded the application of well-established hydraulic geometry relationships or process-based explanatory models due to the difficulties associated with up-scaling (Latrubesse, 2008). Furthermore, the river's complex and dynamic planform has also precluded application of conventional, geometric models developed for simpler, meandering channels (e.g. Ikeda et al., 1981; Parker et al., 1983; Johannesson and Parker, 1989; Zolezzi and Seminara, 2001; Camporeale et al., 2005). In fact, the difficulty inherent in large-scale, long-term studies of channel evolution and bank line migration in complex, multi-channel rivers prior to the wide availability of high definition, remotely sensed imagery explains why such studies have, until recently, been rarely conducted (Best and Bristow, 1993; Richardson, 1997). To date, the majority of geomorphological studies of the Jamuna have instead focused on investigating the processes responsible for channel evolution and bank line migration at the scale of the individual geomorphological unit. Examples include studies of channel bifurcations and braid bars (Ashworth et al., 2000; Richardson and Thorne, 2001); braid bars and associated floodplain embayments (Thorne et al., 1993; Halcrow, 1994) and the evolution of meander bends in major anabranches (Thorne and Russell, 1993; Ellis, 1993).

The bank line adjustment processes associated with these different geomorphological units exhibit non-stationarity (spatial and temporal localization) as well as different, characteristic bank migration rates and scale-dependency in space (circa  $10^2 - 10^4$  m) and time (circa  $10^0 - 10^1$  yr). It follows that, in rivers with multi-channel planforms, the overall pattern of bank retreat is characterized as a complex non-stationary waveform within which multiple, characteristic erosion patterns co-exist at different scales, and at different downstream locations. For example, Thorne et al. (1993) identified a gross-scale control of planform evolution associated with island and

nodal reaches first described by Coleman (1969) that are spaced along the channel at intervals of circa 30 km. They also identified local bank migration processes that are driven by braid bar growth and migration and which operate at smaller spatial (3 - 6 km) and over shorter temporal scales (2 - 5 years). Their findings contrast with those of Ellis (1993), who observed bank erosion and embayment formation related to meander growth and migration in near-bank anabranches that occur at spatial scales of hundreds of metres to several kilometres, persist over periods of 1-12 years, and drive erosion rates ranging from 50 to over 250 m yr<sup>-1</sup>. More recently, CEGIS (2007) identified bank erosion and floodplain embayment forming processes associated with bar form development in the Jamuna river operating at spatial scales of 3-15 km, over periods of approximately 15 years and with erosion rates of the order of 200 m yr<sup>-1</sup>. A finding common to these studies was that rates of downstream migration in the locations of severe bank erosion also appear to be scale-dependent. This is consistent with the downstream movement of sand bars (Coleman, 1969) and changes in the location of relatively stable and unstable reaches over time (Takagi et al., 2007), which all suggest a link to the downstream propagation of sediment waves (Gilbert, 1917; Madej and Ozaki, 1996; Wathen and Hoey, 1998). Indeed both Thorne et al. (1993) and Takagi et al. (2007) identified wave-like patterns of channel migration, with characteristic wavelengths of ~150 km and ~35 km, respectively. These findings suggest that the complex patterns of bank retreat observed in the Jamuna result from the superimposed and cumulative effects of spatially-transient bank erosion processes, operating semi-independently at a range of spatial and temporal scales.

Marcus and Fonstad (2010) argue that the development and availability of new remote sensing technologies, coupled with widening accessibility to GIS, have led to the emergence of the 'remote sensing of rivers' as a sub-discipline of fluvial geomorphology. Complex patterns of bank migration are now commonly investigated based on temporal sequences of bank line data, captured from aerial photographs or remotely-sensed imagery. These data are analysed within a geographical information system (GIS) so

that rates of bank line retreat during specified periods can be computed (e.g. Gurnell et al., 1994; Mount et al., 2003; Mount and Louis, 2005; Swanson et al., 2011). In such studies, characterisation of downstream migration in bank erosion patterns reduces to a problem of localizing in space the different magnitudes and scales of bank retreat events that can be discerned from the data, and evaluating how these localized patterns vary through time. In the past this has been achieved through a largely qualitative, visual appraisal of the patterns observed in sequential plots of bank position or change (e.g. Downward et al., 1994; Gurnell, 1997; Mount et al., 2003) coupled with examination of summary bank retreat statistics (e.g. CEGIS 2000; 2007). Consequently, relatively little quantitative understanding of either trends in the spatial localization associated with erosion at different scales or the relative rates of erosion driven by the different processes represented in the bank retreat record has been achieved. Moreover, it has been difficult to causally relate the observed patterns of bank retreat to likely geomorphological drivers; especially where these involve processes acting at different spatial and temporal scales. Commenting on this in a recent review, Kleinhans (2010) acknowledged the potential of remotely sensed time-series for unravelling channel pattern changes, but also observed that, 'we need quantifiers for subtle patterns to reveal structure objectively' (Kleinhans, 2010; page 313).

A more quantitative approach involves viewing the downstream distribution of bank retreat as a spatial signal of planimetric change. According to this approach, the different scales of erosion are equivalent to the different frequencies contained within the signal and their magnitudes are equivalent to signal amplitude. Accordingly, the downstream signal of erosion becomes the spatial equivalent of a standard time series signal, with distance substituted for time. When re-conceptualised in this way, techniques developed for the characterisation of frequency and amplitude in complex signals, become potentially powerful tools for characterising bank retreat. One common tool is the fast Fourier Transform (FFT), which offers good frequency localisation albeit at the expense of poor spatial localisation (Graps, 1995). However, the FFT requires the

data series to be consistent with a statistically stationary model – something that cannot necessarily be assumed when analysing bank retreat sequences in river channels (Van Gerven and Hoitink, 2009). Alternative methods offering *both* frequency and spatial localization, such as the windowed Fourier transform (WFT) (also known as the short-time Fourier transform) and wavelet analysis are therefore, preferable. Both have been applied to the analysis of river patterns (Ferguson, 1975; Camporeale et al., 2005, Van Gerven and Hoitink, 2009). However, the WFT is considerably less adaptable than wavelet analysis in that achieving good spatial resolution requires sacrificing frequency localisation, and *vice versa* (Fournier, 1995 page 11). As a result WFT was not selected for use in this research. While the use of wavelet analysis by geomorphologists remains rare, it has been widely used by hydrologists for the characterisation of runoff time series (e.g. Brillinger, 1994; Fraedrich et al., 1997; Labat et al., 1999, 2000, 2002; Compagnucci et al., 2000; Gauchere, 2002; Lafreniere and Sharp, 2003; Coulibaly and Burn, 2004; Labat, 2005) Also, its potential in analysing signals in time series of river planform change has recently been recognised by Van Gerven and Hoitink (2009), who used it to characterise meander geometry on the Mahakam River, Indonesia. There are, however, no published examples of its use in characterising bank migration in large rivers with anabranching planforms.

In this paper we explore the potential of the continuous wavelet transform (CWT) for the quantitative characterisation of temporal sequences of downstream bank line migration patterns, using data recorded along a 204 km reach of the Jamuna River, Bangladesh. The CWTs presented in this paper quantify changes in bank position in the plane of maximum bank erosion. In line with previous studies of planform change from remotely-sensed data, this is assumed to be orthogonal to the downstream direction. This is believed to be the first time such an approach has been applied in a bank line retreat study. In section 2 we describe the CWT method. Section 3 presents the geomorphologic application, results and interpretation of the CWT to patterns of bank

line retreat on the Jamuna River. The key findings from the study are summarised in section 4.

## 2. Methodology

Wavelet analysis comprises several mathematical transforms from which temporal (or spatial) series can be transformed into a 2-D time (or space)-frequency representation. A detailed treatment of the mathematics of wavelet transforms is beyond the scope of this paper, but may be found in publications covering both wavelet analysis theory (see Daubechies, 1992) and software implementation (Nason, 2008). In this paper we make use of the continuous wavelet transform (CWT) popularised by Torrence and Campo (1998). Our description of the CWT below draws from Torrence and Campo (1998) using the notation and development of Sadowsky (1996), Kumar and Foufoula-Georgiou (1997), and Biswas and Si (2011). In this description,  $y(x)$  denotes the spatial series of left bank (LB) downstream distance measurements. We can define the CWT, which we denote by  $W(s, \sigma)$ , as the complex conjugation of  $y(x)$  with a dilated and translated 'mother' wavelet function  $\psi_{s,\sigma}(x)$ :

$$W(s, \sigma) = \int_{-\infty}^{\infty} y(x) \overline{\psi_{s,\sigma}(x)} dx$$

(1)

where

$$\psi_{s,\sigma}(x) = \frac{1}{\sqrt{s}} \psi\left(\frac{x - \sigma}{s}\right)$$

(2)

Here,  $s$  represents the dilation (scale) of the wavelet function and  $\sigma$  represents the degree of distance translation along the series. The term  $1/\sqrt{s}$  normalises the wavelet function energy at each scale (Kumar and Foufoula-Georgiou, 1997; Torrence and

Campo, 1998). Equation (2) emphasises that the wavelet function is in fact a 'basis' function (Fournier, 1995). For the CWT of a discretely sampled spatial series denoted by  $W_D(s)$  for a distance index  $d$  the integral in Equation (1) is substituted by a summation and the distance  $x$  is replaced by increments of size  $\delta x$  (Torrence and Campo, 1998; Gurley and Kareem, 1999; Biswas and Si, 2011). Finally, the wavelet power spectrum for a given transform can be defined as  $|W_D(s)|^2$  (Torrence and Campo, 1998; Biswas and Si, 2011).

Wavelet functions are required to have a compact support (in other words they decrease rapidly to zero) and a mean of zero (Farge, 1992; Kumar and Foufoula-Georgiou, 1997). In spite of these requirements, there are a great number of functions available which satisfy these criteria. These can be classified in various ways such as (a) orthogonal or non-orthogonal; (b) complex or real and in terms of (c) width and (d) shape (see Torrence and Campo, 1998 § 3e). *Non-orthogonal* wavelets (they overlap) are used in the CWT. The CWT therefore incorporates considerable redundancy in the representation of the spatial series (Kumar and Foufoula-Georgiou, 1997) and an alternative to this is to make use of *orthogonal* wavelets which are the basis of the discrete wavelet transform (DWT) which in its simplest form can be thought as a set of slices through the CWT at scales defined by powers of two (Percival et al., 2004). However, it is argued that the non-orthogonal wavelets as used in the CWT are possibly more appropriate for spatial series analysis as they can reveal more information on scale localization (Biswas and Si, 2011). Non-orthogonal versions of the DWT do exist such as the maximal overlap discrete wavelet transform and maximal overlap discrete wavelet packet transform which have also been applied in the analysis of spatial series (Milne et al., 2010).

Common examples of complex non-orthogonal wavelets used in the CWT (and the focus of Torrence and Campo, 1998) include the Morlet (Fig. 1 A,B, Equation 3) and the Paul (Fig. 1 C , Equation 4) wavelets, whilst the Derivative of Gaussian (DOG) (Fig. 1



206 D, Equation 5) is an example of a real-valued function (equations modified from  
207 Torrence and Campo, 1998):

$$\psi(x) = \pi^{-1/4} e^{ikx} e^{-x^2/2}$$

208 (3)

$$\psi(x) = \frac{2^k i^k k!}{\sqrt{\pi(2k)!}} (1 - ix)^{-(k+1)}$$

209 (4)

$$\psi(x) = \frac{(-1)^{k+1}}{\sqrt{\Gamma(k + \frac{1}{2})}} \frac{d^k}{dx^k} (e^{-x^2/2})$$

210 (5)

211 Here,  $k$  is the parameter (known as the wavelet order) that controls the number of  
212 oscillations in the wavelet function with the result of altering the resolution (both  
213 frequency and distance) of the wavelet transform (De Moortel et al., 2004).

214 The choice of the most appropriate mother wavelet function to use in a wavelet  
215 analysis (along with the optimal value of  $k$ ) depends largely on the characteristics of the  
216 signal itself, ideally reflecting the shapes of features present in the data series to be  
217 analysed (Lane, 2007). However, there is a distinct lack of advice in the wavelet  
218 literature on the optimal choice of these parameters, leading to the development of  
219 context dependent criteria for relative comparison (e.g., Fu et al., 2003) which may or  
220 may not be universal. Although Torrence and Campo (1998) have suggested that  
221 different functions will nevertheless give the same qualitative results for wavelet power  
222 spectra (Torrence and Campo, 1998), the practical advice of De Moortel et al. (2004) to  
223 experiment with different parameters would seem appropriate.

224 *2.1. Cone of influence and significance levels*

As noted by De Moortel et al., (2004) the CWT as implemented in code such as that developed by Torrence and Campo (1998) is often speeded up by transforming to Fourier space. Common to Fourier transforms of finite series this introduces edge effects primarily due to 'spectral leakage' as a result of edge discontinuities (Fougere, 1985). There are a variety of methods to ameliorate such effects: the approach taken in Torrence and Campo (1998) is 'zero padding' whereby zeros are added to the data series up to the next integer power of two. This results in a 'cone of influence' (COI) at the margins of the wavelet transform where the interpretation of the wavelet transform should be considered unreliable (De Moortel et al., 2004).

It is also possible to perform a statistical significance test and calculate significance by comparing the wavelet power to an appropriate background noise spectrum. Commonly, either white noise or red noise (increasing power with decreasing frequency) are used with the latter being a more realistic model of many geophysical series that exhibit short distance spatial dependence (see Fougere, 1985). Red noise is therefore often preferred (e.g., Si and Farrell, 2004 and references therein) and can be modelled by a first order autoregressive AR(1) process (modified from Torrence and Campo, 1998):

$$x(t) = c + \alpha x(t - 1) + z(t)$$

(6)

Where  $c$  is a constant,  $\alpha$  is the lag-1 autocorrelation and  $z(t)$  is white noise. We refer the interested reader to the description of the Fourier power spectrum of (6) and a full explanation with formulae for the quantification of significance levels using a Monte Carlo simulation approach to Torrence and Campo (1998; § 4) as well as a summary treatments by Si and Farrell (2004). If a peak in the wavelet power spectrum is significantly above this background we might ascribe this to a scale dependent pattern/process operating at that frequency. In this study we use a red noise

background spectrum with  $\alpha$  computed according to the AR(1) coefficient and present all significant results using the 95% confidence level.

## 2.2. Scale-averaging wavelet spectra

The fluctuations in wavelet power across discrete scale ranges or bands can be achieved by defining the *scale-averaged wavelet power* as the weighted sum of the wavelet power spectrum over scales  $s_1$  to  $s_2$  (modified from Torrence and Campo, 1998; Coulibaly and Burn, 2004):

$$\bar{W}_D^2 = \frac{\delta j \delta x}{C_\delta} \sum_{j=j_1}^{j_2} \frac{|W_D(s_j)|^2}{s_j}$$

(7)

where  $C_\delta$  is a constant that can be derived for any wavelet function via reconstruction, and  $\delta j$  depends on the width of the wavelet function used and should ensure adequate sampling in scale (see Torrence and Campo, 1998 § 5b for the derivation formulae). Significance levels can also be ascribed to the scale averaged wavelet power via an analytical relationship between the significance levels and the scale-averaged wavelet power. For details of this the reader is again directed to Torrence and Campo (1998). The scale averaged wavelet power is a series of the average variance in a certain band. It can, therefore, be used to examine modulation of one series by another and / or modulation of one frequency series by another within the same series.

## 3. Geomorphologic application: bankline retreat characterisation of the Jamuna River

In this study we analyse bank migration along a 204 km reach of the Jamuna river in Bangladesh (Fig. 2), between its confluence with the Teesta River just south of the Indian border, and the Ganges River. The Jamuna is one of the largest and most dynamic rivers in the world ranking fifth in terms of discharge (mean flow 12,200

cumeecs) and eleventh in terms of drainage area (666,000 km<sup>2</sup>) (Thorne et al., 1993). Analysis of the long-term evolution of the channel (Coleman, 1969; Burger et al., 1991; Thorne et al., 1993; ISPAN, 1995; CEGIS, 2001; Takagi et al., 2007) has revealed a highly dynamic channel that has undergone westward migration, widening and planform metamorphosis following the creation of the present river by avulsion in 1830. The meandering planform of the 19th century channel has been replaced by a much wider, braided channel throughout the 20th century, and this change has been accompanied by very high rates of bank line retreat. In the last three decades, the majority of this retreat can be related to channel widening rather than centreline migration, although the left hand bank does show a slightly higher average retreat rate (68 m yr<sup>-1</sup> between 1973 and 2000) than the right hand bank (60 m yr<sup>-1</sup>) (CEGIS, 2000).

In this study we concentrate our analysis on patterns of bank retreat occurring between 1987 and 1999. This period is characterised by particularly rapid channel widening with spatially-variable and non-stationary patterns of stabilisation / destabilisation; possibly associated with propagating sediment waves (Thorne et al., 1993; Takagi, 2007), related to sediment supplied from upstream by the 1950 earthquake in Assam (Goswami et al., 1999). The pattern of bank retreat evidences erosion at a wide range of scales from individual embayments to island reach scales. The existence of localised, multi-scale bank retreat patterns, coupled with high retreat rates make the period particularly well suited to wavelet analysis.

The floodplain of the left-hand bank (LHB) is comprised of newly accreted land which is characterised by poorly consolidated and easily eroded bank material. This has resulted in much more localised and complex patterns of bank retreat than that of the right-hand bank (RHB) (Thorne et al., 1993). Indeed, between 1973 and 2006, 49,460 hectares of land eroded along 190 km of LHB, compared to 38,540 hectares along 245 km of RHB (CEGIS, 2007). Similarly, maximum rates of erosion are highest on the LHB with local erosion exceeding 2000 m yr<sup>-1</sup> in several locations. As a consequence, the downstream pattern of bank retreat for the LHB is characterised by events of greater

amplitude, greater variability of scale and greater spatial variability than the RHB, and we have therefore selected the LHB data for subsequent analysis in this study.

### *3.1. Bank line delineation methods and data series*

The data used in this study have been sourced from the Centre for Environmental and Geographical Information Services (CEGIS), Dhaka. CEGIS have been responsible for quantifying bank retreat rates along the entire length of the Jamuna in Bangladesh from satellite imagery for the period 1973 – present. Their data has formed the baseline geomorphological dataset for the World Bank’s Flood Action Plans (FAP-1, 1991; 1992). We provide a summary below of the methods used to generate the data – further details can be obtained from CEGIS (1997, 2001), including information on ground validation of satellite image analysis.

A time-series of dry season Landsat MSS and TM images were used to document historical changes in LHB position along the study reach. The time series of images covered the period 1987-1999 (Table 1), allowing LHB migration to be computed for 8 separate periods: 1987-89; 1989-92; 1992-94; 1994-95; 1995-96; 1996-97; 1997-98 and 1998-99. All images were mosaiced and georeferenced to a 1:50,000 scale colour base map; originally derived from 1989 high resolution SPOT satellite images, and projected using the UTM-46N projection (CEGIS, 2007). For each image in the mosaic, more than 25 ground control points were used to define a first order transformation to the base map. Where possible, ground control points were taken from recognizable and permanent features such as road intersections, airport runways and large buildings. The maximum root mean square (RMS) error of the transformation was 96 m for the Landsat MSS imagery (1987) and 45 m for the Landsat TM imagery (1989-1999).

The Jamuna in Bangladesh flows approximately due south (Fig. 2), and the channel is therefore orientated along a consistent northing ordinate throughout its length. Following the established methods of Gurnell et al. (1994); Gurnell (1997); Mount et al. (2003) and Mount and Louis (2005) maximum bank erosion in the Jamuna can therefore

be assumed to occur in a direction orthogonal to the main channel (i.e. in an easterly direction). Bank line position was assessed at a downstream spacing of 500 m; defined by each image's northing coordinate. Consequently, LHB migration between consecutive images at each downstream location was computed as the difference in the easting coordinate of the bank line position, converted to  $\text{m yr}^{-1}$  according to the capture dates of the imagery (Table 1). Bank lines were defined as the line which separates the floodplain from the active braid belt. In general, bank lines encompass main channels, island chars and sand bars in the river braid belt, except for crevasse splays (the coarse sediments that are spread over the floodplains during floods). Where a major anabranch of the river flows along the edge of the floodplain in a channel (which typically ranges in width from hundreds of meters to several kilometres), the bank line delineation is simple and uncontroversial. However, smaller distributary channels flowing next to the bank are more difficult to define and a number of criteria can be applied to determine whether they should be considered a part of the active braid belt (CEGIS, 1997, 2000):

- (1) channels are outside the bank line if the channel does not return to the main river;
- (2) channels are outside the bank line if the channel is less than 100 m in width;
- (3) channels are outside the bank line if the channel has a meander radius of less than one kilometre.

Due to the difficulties associated with determining whether material deposited at the channel margins between images remains active channel or has become incorporated into the floodplain, only bank line retreat rates are recorded in the data series (deposition is recorded as zero). This means that the analysis presented here represents a partial examination of the patterns on planimetric change on the Jamuna, which comprise both bank line retreat and bank advance; the latter occurring through the incorporation of sediments previously considered to be within the active channel into the floodplain. All bank line retreat between consecutive images of 50 m or less was considered to be within the margin of measurement and georeferencing error and was

recorded as zero retreat. For the periods 1989-92, 1992-94; 1994-95; 1995-96; 1996-97; 1997-98 and 1998-99, where all images are of 30 m resolution, this margin exceeds the 42 m quadratic sum associated with a ground feature identification error of  $\pm 1$  pixel in each image (c.f. Mount and Louis, 2005). For the period 1987-89, in which one 30 m and one 80 m resolution image are used, this value is less than the 85 m quadratic sum of the  $\pm 1$  pixel ground feature identification error. Consequently, the magnitude of bank line retreat in this period may be slightly over-estimated in the data. In addition to the bank line data, daily mean discharge records from Bahadurabad ( $21.15^{\circ}\text{N}$ ,  $89.70^{\circ}\text{E}$ ) were also acquired from CEGIS. The resultant temporal sequence of bank line retreat series is provided in Figure 3.

### *3.2. Wavelet function selection*

In this study we consider the three wavelet functions described in Torrence and Campo (1998) and detailed in Equations (3-5). These three functions offer a range of different localisation capabilities (which are described in detail in De Moortel et al. 2004). The Morlet wavelet (Equation 2) offers high frequency localisation capabilities which result from the presence of a large number of oscillations but this increases the wavelet width which in turn reduces spatial localisation capability. The Paul (Equation 3) wavelet offers higher spatial resolution (it has fewer oscillations), but at the expense of frequency localisation. The DOG (Equation 4) offers excellent spatial localisation of individual peaks in the series, but can suffer from discontinuity in the frequency localisation in the transform.

To assist in the identification of the preferred wavelet, a CWT decomposition of the 1998-99 bank line retreat data was undertaken using all three wavelet functions using the software developed by Torrence and Campo (1998) and implemented in MATLAB. The 1998-99 data was selected because it represents one of the more complex data series in the temporal sequence with a wide range of spatial scale and magnitudes of bank line retreat evident. The relative lack of local oscillation complexity in the bank

line retreat series implies adequate frequency localisation should be achieved with a relatively low wavelet parameter ( $k$ ) value. Moreover, the use of a small value of  $k$  reduces the area of the transform under the COI. Therefore,  $k$  was set to 3. However, a transform was also generated using a Morlet,  $k = 6$  wavelet to determine the impact of increasing the  $k$  value. The results are provided in Figure 4.

The Paul  $k=3$  and Morlet  $k=3$  wavelets can be seen to generate very similar patterns of significant wavelet power, associated with the same local peaks of bank line retreat. There are subtle differences between the two in terms of their space / frequency localisation capabilities. The Morlet  $k=3$  transform exhibits some horizontal compression and increased lateral connectivity of the 95% confidence regions in comparison with the Paul  $k=3$  transform; thereby highlighting its greater frequency localisation capabilities. The DOG wavelet can be seen to localise peaks particularly well, but at the expense of frequency. The result is lateral discontinuity in the 95% confidence regions (which is also reported in De Moortel et al., 2004) and a frequency localisation that is difficult to interpret. Increasing the Morlet wavelet  $k$  value to 6 results in a larger COI and a loss of significant wavelet power regions at high frequencies and the loss of spatial localisation (i.e. the 95% confidence regions elongate horizontally); thus making it difficult to map the significant bank line retreat frequencies accurately on the ground. The results indicate that both the Paul  $k = 3$  and Morlet  $k = 3$  represent appropriate wavelet functions for the bank line retreat data series. However, in this paper we use the Morlet  $k = 3$  wavelet on the basis that it provides enhanced frequency localisation with minimal loss of spatial localisation.

### *3.3. Results*

#### *3.3.1. Continuous wavelet transform spectra*

The CWT spectra for the 8 bank line retreat series (Fig. 3) calculated using an adaptation of the Torrence and Campo (1998) code are presented in Figure 5. Regions



of wavelet power that exceed the 95% confidence level are those within the bold lines, with the dashed line indicating the COI.

The CWT spectra highlight two characteristic groupings of bank line retreat patterns over the study period. Zones of significant wavelet power in 1996-97; 1997-98 and 1998-99 are largely constrained to wave periods of 16 km or less. These comprise a mixture of small, very short wave periods (1-4 km) with very high spatial and frequency localisation and a broader range of wave periods (2-16 km) in which the spatial and frequency localisation is less well resolved. At both wave periods, significant zones are spatially discrete and separated by downstream distances of between 10 and 20 km. Moreover, there appears to be some temporal persistence in their location. Such patterns are characteristic of locally-persistent bank line retreat events which occur independently of any larger bank line retreat process (i.e. there is little evidence of local bank line erosion patterns being superimposed on larger-scale, regional patterns). In certain cases, the retreat is highly constrained to within a very short stretch of bank (i.e. the 1-4 km wave period regions), whereas in others longer stretches are implicated (2-16 km period regions).

By contrast, zones of significant wavelet power in 1987-89; 1989-92; 1992-94 1994-95 and 1995-96 are characterised by the existence of longer wave periods (16-64 km) extending over substantial downstream distances. These are coupled, to varying extents, with superimposed and locally-discrete short wave period zones, which are similar in character to those of 1996-97; 1997-98 and 1998-99, but less numerous. Importantly, there is some evidence of downstream movement in the locations of the longer wave period significance zones, from 0 – 60 km in 1987-89; 40 – 80 km in 1992-94; 60 – 100 km in 1995 to 95 and 100 – 160 km in 1995-96. Such patterns are difficult to interpret, yet their characteristic long wave periods, coupled with substantial downstream extension and translation, would indicate that they may be characteristic of bank retreat driven by the passage of a sediment-wave, or linked to the presence of large, island char (quasi-stable, mature, vegetated islands within the active channel belt).

### 436 3.3.2. *Scale averaging*

437 Each of the CWTs was scale averaged into 0-10 km and 10-30 km bands  
438 according to the scales of the two major downstream controls of bank retreat pattern  
439 identified as operating on the Jamuna (c.f. Thorne et al., 1993). The 0-10 km band  
440 encompasses the scale of individual braid-bars responsible for local bank retreat due to  
441 embayment (CEGIS, 2007) and local bend evolution (Ellis, 1993). The 10-30 km band  
442 encompasses the scale of island / nodal reaches associated with lower frequency  
443 patterns of bank retreat governing gross-scale planform evolution (Thorne et al., 1993),  
444 and the wavelength of propagating sediment waves (Takagi et al., 2007). The  
445 downstream pattern of scale-averaged wavelet power exceeding the 95% confidence  
446 level for each time period is plotted onto a single graph for each scale range (Fig. 6).  
447 This allows the spatial and temporal persistence of different scales of bank retreat to be  
448 investigated. Because the 95% confidence level of the scale-averaged wavelet power  
449 varies between each time period, y-axis values are standardised as multiples of the 95%  
450 confidence level for each retreat period.

451 At the 0-10 km scale, the LHB can be separated into a number of clearly defined  
452 reaches according to the magnitude (i.e. the wavelet power multiples above the 95%  
453 confidence level) and spatio-temporal persistence (i.e. the number of consecutive years  
454 wavelet power exceeds the 95% confidence level at a given location) of the bank retreat  
455 patterns (Table 2). Three low-magnitude, stable reaches, which exhibit little or no  
456 significant wavelet power at scales of 0-10 km, at any time period, are visible at ~57-65  
457 km, ~120-135 km and ~155-164 km. The last of these is almost certainly related to the  
458 existence of stable guide bunds for Jamuna Bridge (Fig. 2). In all cases, these stable  
459 reaches are short; not exceeding 15 km in length. In contrast two reaches exhibit  
460 persistent significant 0-10 km wavelet power throughout the majority of the study period,  
461 which is, at times, of high magnitude. These are located at ~65-85 km and ~135-155  
462 km. They represent reaches of moderate length (~20 km), which exhibit consistent and  
463 substantive bank line migration operating at scales indicative of embayment and

meander bend processes. Importantly, there is little evidence of downstream translation of bank line retreat with the locations of each of the main peaks in wavelet power occurring within  $\sim 10$  km of each other (i.e. within the bounds of the spatial localisation capabilities of the Morlet  $k=3$  mother wavelet). Between these two end members are a further three reaches in which the spatio-temporal pattern of bank retreat is transient and of variable magnitude. These reaches range in length from 18 - 39 km. Importantly, the transient reaches show clear evidence of downstream translation of the peaks in wavelet power, as indicated by arrows in Figure 6. This may imply the presence of transfer reaches where sediment eroded from the persistent, high magnitude reaches is transferred downstream; instigating localised bank retreat as it is transported.

At the island / node reach scale (10-30 km) there is little temporal persistence in the locations of peak wavelet power; and thus of bank line retreat. However, the existence of a stable, nodal reach at 100 - 120 km is of note. There is clear evidence of downstream propagation of bank retreat. Between 1987-89 and 1995-96 a consistent downstream translation of the peak wavelet power is visible, from  $\sim 25$  km to  $\sim 75$  km, and at a mean annual rate of approximately  $8 \text{ m yr}^{-1}$ . This pattern is consistent with that of sediment wave propagation observed by Takagi et al. (2007), both in terms of its scale and location.

The temporal analysis presented in Figure 6 provides a simplified appraisal of the pattern of location and frequency variation in bank retreat through time, where the complexity has been reduced through the temporal isolation of the scale-averaged power spectra from each CWT. As a result, the analysis does not provide a detailed evaluation of the patterns of covariance from one CWT to the next. Techniques such as cross-wavelet transforms and wavelet coherence analysis (Grinsted et al., 2004), that specifically focus on quantifying the covariance between sequences of CWTs, offer considerable potential in this regard (Torrence and Webster, 1999). Whilst the

application of these advanced techniques is beyond the scope of this paper, their importance as a direction for future research should be recognised.

### *3.3.3. Wavelet power relationship to discharge*

One of the key challenges in geomorphologic studies has been establishing and elucidating the relationships between processes operating over different temporal and spatial scales (Rhoads and Thorn, 1996, pp. 145-6; Phillips, 1999a,b; Couper, 2004). Wavelet decomposition of sequential geomorphologic signals offers potential in this regard through the examination of the pattern of variability in the strength of the wavelet power at different frequency localisations and time periods and its relationship with potential physical drivers of the signal.

To this end, we also examine the relationship between different scales of bank retreat and discharge by quantifying the definite integral of the downstream scale-averaged wavelet power spectra each time period (i.e. a numerical proxy for the total magnitude of LHB retreat occurring at that scale) and plotting this against two measures of peak discharge: the maximum discharge and the  $Q^{95}$  exceedance period (Table 3). Whilst maximum discharge is identified as an important driver of bank retreat (Sarker and Thorne, 2006; CEGIS, 2007), the use of variable time periods in this study means that a time-integrated measure of peak discharge (i.e.  $Q^{95}$  exceedance) should also be included in the analysis.

The CWT for each time period was scale-averaged into the following regular intervals: 0-10 km; 10-20 km; 20-30 km; 30-40 km; 40-50 km. The definite integral of each of the scale-averaged spectra for each time period was then quantified using the trapezoidal rule and plotted against the peak discharge measures determined from the available discharge records at the gauging station at Bahadurabad (Fig. 7).

At 0-10 km and 10-20 km scales, strong positive, exponential relationships are seen to exist between the integral of the wave power spectrum and  $Q_{Max} / Q^{95}$  exceedance (Figs. 8 and 9). This indicates that as peak discharge increases, so too does

the total amount of bank retreat on the LHB of the Jamuna. It is interesting to note that, in general, the strength of the relationships is stronger for maximum discharge than for  $Q^{95}$  exceedance, suggesting that QMax may be a more useful peak discharge parameter when attempting to predict bank retreat on the Jamuna. Positive relationships also exist at larger scales, albeit with far lower integrated power spectrum values, and lower Pearson coefficients. The positive relationships identified are not unexpected as the mean rate of bank retreat on the Jamuna is known to be related to the magnitude of the largest monsoon flood (Sarker and Thorne, 2006; CEGIS, 2007). However, the evidence that the strength of the relationship shows a consistent decrease as scale increases is new and important knowledge. Overall reductions in the magnitude of the wavelet power spectrum integrals are accompanied by a reduction in  $R^2$  values as scale increases. For QMax the reduction is from 0.86 at 0-10 km scales to less than 0.5 at scales greater than 30 km. For  $Q^{95}$  exceedance the reduction is from  $\sim 0.5$  at scales less than 20 km to  $\sim 0.3$  at scales greater than 40 km. Thus, the pattern is one in which peak discharge is strongly related to the rate of bank retreat on the Jamuna, but only at spatial scales of less than 20 km. As the scale of bank retreat increases the importance and statistical significance of peak discharge as a main driver of bank retreat is substantially reduced.

#### *3.4. Geomorphologic interpretation*

A number of key characteristics of bank line retreat on the LHB of the Jamuna river have been identified through the CWT analyses presented. Whilst some can be interpreted with reference to well-understood geomorphologic processes and conventional geomorphological thinking, others are more difficult to interpret and further work is required to provide an adequate geomorphological explanation.

The CWT sequence in Figure 5 shows that at different times in the Jamuna river data series varying amounts of significant, short (2-16 km), moderate (16-32 km) and long (>32 km) wave-period bank retreat are evident. In some years (e.g. 1996-97;

1997-98 and 1998-99), spatially-discrete regions of short wave-period bank retreat are dominant and there is little evidence of significant retreat at longer periods. This indicates that, at these times, the main mode of planform adjustment is local; through the erosion of individual embayments. At other times (e.g. 1987-89; 1989-92; 1992-94; 1994-95 and 1995-96) the co-existence of significant regions of wavelet power at longer wave-periods indicates that a regional mode of planform adjustment at or above the scale of individual chars operates is also in operation. Indeed, in some years (1994-95 and 1995-96) significant regions of bank retreat at long wave-periods strongly suggest a macro-scale model of adjustment that exceeds the scale of individual island chars.

The scale-averaged data presented in Figure 6 are more easily interpreted and provide important geomorphological insights into the different characteristics of the spatio-temporal patterns of bank retreat operating at different scales. At scales of 0-10 km the evidence of locally-persistent retreating banks, separated by stable and/or transient reaches, corresponds well with the findings from other studies of local embayment patterns on the Jamuna (Ellis, 1993). However, the precise reasons for the alternating pattern of stable / transient / eroding reaches at this scale are not fully understood. At the scales at which gross planimetric control of bank retreat by quasi-stable island / node reaches (10-30 km) is thought to dominate (Coleman, 1969; Thorne et al., 1993) there is relatively little evidence that the locations of significant bank retreat can be mapped directly to the locations of island reaches. Indeed, Thorne et al., (1993) identify seven separate island and nodal reaches located at roughly regular downstream spacing throughout the 204 km study reach. However, no evidence of such spacing in the pattern of significant bank retreat is evident in Figure 6, and only one persistently stable reach is evident. This suggests that the importance of island and nodal reaches on influencing the pattern and magnitude of bank retreat at large spatial scales may be less important than previously thought. Instead, the downstream propagating patterns of retreat observed correspond more closely to the influence of sediment waves; the importance of which has been recognised in earlier studies (Takagi

et al., 2007). Indeed, they estimated a wavelength of 35 km and found the best evidence for the propagation between 10 and 80 km downstream - approximately the same wavelength and location of the patterns observed in Figure 6. Thus, additional support is provided to the implication that propagating sediment waves are important drivers of bank retreat patterns operating at scales of tens of kilometres on the Jamuna.

Relating the integral of a range of scale-averaged wavelet power spectra to maximum discharge and  $Q^{95}$  exceedance, Figures 8 and 9 provide an important and explicit confirmation of conventional geomorphological thinking about the importance that can be ascribed to peak discharge as a driver of bank migration at different scales (e.g. Hooke, 1980; Nanson and Hickin, 1986). On the LHB of the Jamuna the magnitude of the peak discharge is strongly related to the integral of the wavelet power spectrum at 0-10 and 10-20 km scales and, hence, the magnitude of erosion at frequencies that coincide with meander bend and embayment processes. At lower frequencies, where the gross planimetric setting and regional factors such as the spatial variability of floodplain substrate cohesiveness become important constraints on erosion, the relationship between measures of peak discharge and wavelet power decreases.

#### **4. Summary and conclusions**

The Jamuna river provides an important venue for fundamental research on process-form interactions in large-scale, complex fluvial systems. It is the epitome of a wilful stream representing a complex, non-linear, dynamical system within which fluvial processes, morphological responses and process-response feedback loops operate at multiple scales of time and space. Past efforts at understanding this system have generally focussed on studying the processes governing the evolution of individual geomorphological units operating at a single scale within the channel, (e.g. anabranches, bars, bends and bifurcations within the braided system). Yet, their value in understanding how the system operates across its whole range of scales and periods of adjustment are unavoidably limited by the approaches taken. As a consequence, the

600 multi-scale explanatory linkage between fluvial processes and channel evolution  
601 envisaged first by Schumm and Lichty (1965) and later by Lane and Richards (1997)  
602 remains poorly developed.

603 CWTs offer an important means by which key signals of planimetric change, in  
604 the case of this study captured as sequences of bank migration spatial series, can be  
605 localised not only in time, but also in space. This offers a powerful means of  
606 characterising where, when and over what spatial scales change occurs. It thus  
607 represents the first, vital step in determining a multi-scale, explanatory framework for  
608 relating channel process and channel pattern evolution. In many cases, it will be  
609 possible to map the patterns observed to the results of past channel evolution process  
610 studies. In this context, CWTs offer an important means of identifying spatio-temporal  
611 patterns of bank retreat at different scales that can then be linked to fundamental  
612 processes of channel adjustment and the findings of past research efforts. In other  
613 cases, the patterns observed in the CWT will be more difficult to explain by conventional  
614 geomorphological thinking. In these cases, CWTs offer an important means by which  
615 new research directions can be identified and directed.

616 However, the outputs from a CWT are only as good as the input data. Indeed,  
617 the selection of a planimetric signal capable of providing an adequate characterisation of  
618 the evolutionary processes of interest is critical. For example, whilst sequences of bank  
619 line retreat series offer important insights into erosion processes, they provide no  
620 information about the temporal, spatial and frequency scales at which deposition occurs.  
621 This means that an important component of channel change processes are  
622 uncharacterised and the links between depositional and erosional channel forms can only  
623 be surmised; not explicitly demonstrated. Similarly, by focussing on a single bank line,  
624 only half of the channel's erosion response is characterised. Consequently, determining  
625 the optimum set of channel response signals to which CWT should be applied in order to  
626 gain a more holistic characterisation of the patterns of channel evolution is a pressing  
627 research need. Also of importance is the quality and comprehensiveness of the data



used. Where the length of the data series is short, the relatively large size of the COI will limit the ability to localise low frequency responses in the data. The downstream resolution of the data will ultimately determine the degree to which high frequency responses can be localised. Similarly, the length of time over which the signal is measured, relative to the return period of the fluvial processes responsible for those changes, may reduce the magnitude of certain responses when the data are converted to annual rates. This in turn will reduce their wavelet power in the CWT and may result in their significance being underestimated.

To conclude, the results presented in the paper represent an early, exploratory investigation of the usefulness of wavelet transformation of signals of planimetric change in complex river systems. Considerable potential for the technique is evident, however numerous questions remain and both wavelet analysis in general and CWT in particular offer considerable opportunities for fruitful future research efforts in unravelling river pattern change.

## **Acknowledgements**

Wavelet software was provided by C. Torrence and G. Compo, and is available at URL: <http://atoc.colorado.edu/research/wavelets/>. NJM and NJT thank the Universities of Nottingham and Leicester for the granting of research study leave coinciding with this research.

653   **References**

- 654   Ashworth, P.J., Best, J.L., Roden, J.E., Bristow, C.S., Klaassen, G.J., 2000.  
655   Morphological evolution and dynamics of a large, sand-braid bar, Jamuna River,  
656   Bangladesh. *Sedimentology* 47, 533-555.
- 657   Best, J.L., Bristow, C.S. 1993., Braided rivers: perspectives and problems. In: Best,  
658   J.L.,Bristow,C.S. (Eds.), Braided Rivers. Geological Society of London Special Publication  
659   75, Geological Society, London. pp. 1–11.
- 660   Biswas, A., Si, B.C., 2011. Application of continuous wavelet transform in examining soil  
661   spatial variation: A review. *Mathematical Geosciences* 43, 379–396.
- 662   Brillinger, D.R. 1994., Trend analysis: time series and point process problems.  
663   *Environmetrics* 5, 1-19.
- 664   Burger, J., Klaassen, G.J., Prins, A. 1991., Bank erosion and channel processes in the  
665   Jamuna River. In: Elahi, K.M., Ahemd, K.S., Mofizuddin, M. (Eds.), Riverbank Erosion,  
666   Flood and Population Displacement in Bangladesh. Riverbank Impact Study,  
667   Jahangirnagar University, Dhaka, Bangladesh.
- 668   Camporeale, C., Perona, P., Porporato, A., Ridolfi, L., 2005. On the long-term behavior  
669   of meandering rivers. *Water Resources Research* 41, W12403.
- 670   Centre for Environmental and Geographical Information Services (CEGIS), 1997.  
671   Morphological Dynamics of the Jamuna River. Water Resources Planning Organization,  
672   Ministry of Water Resources, Government of the People's Republic of Bangladesh, Dhaka.  
673   76pp.
- 674   CEGIS, 2000. Riverine Chars in Bangladesh: Environmental Dynamics and Management  
675   Issues. University Press, Dhaka, 88pp.

676 CEGIS, 2001. Remote Sensing, GIS and Morphological Analyses of the Jamuna River.  
677 Part II. River Bank Protection Project, Bangladesh Water Development Board, Dhaka,  
678 Bangladesh.

679 CEGIS, 2007. Long-term erosion process of the Jamuna river. Centre for Environmental  
680 and Geographic Information Services, Dhaka, 74 pp.

681 Coleman, J.M., 1969. Brahmaputra River. Channel processes and sedimentation.  
682 Sedimentary Geology 8, 129-239.

683 Compagnucci, R.H., Blanco, S.A., Filiola, M.A., Jacovkis, P.M., 2000. Variability in  
684 subtropical Andean Argentinian Atuel river: a wavelet approach. Environmetrics 11,  
685 251-269.

686 Coulibaly, P., Burn, D.H., 2004. Wavelet analysis of variability in annual Canadian  
687 streamflows. Water Resources Research 40, W03105.

688 Couper, P.R., 2004. Space and time in river bank erosion research: a review. Area 36,  
689 387-403.

690 De Moortel, I., Munday, S., Hood, A. W., 2004. Wavelet analysis: the effect of varying  
691 basic wavelet parameters. Solar Physics 222, 203-228.

692 Daubechies, I., 1992. Ten Lectures on Wavelets. Society for Industrial and Applied  
693 Mathematics, Philadelphia. 357 pp.

694 Downward, S.R., Gurnell, A.M., Brookes, A., 1994. A methodology for quantifying river  
695 channel change using GIS. In: Olive, L.J., Loughran, R.J., Kesby, J.A. (Eds.), Variability  
696 in Stream Erosion and Sediment Transport, Proceedings of the Canberra Symposium  
697 1994, IAHS Publication No. 224, IAHS Press, Wallingford, pp. 449-456.

698 Ellis, L., 1993. River Bank Erosion and Different Hydrologic Regimes. Unpublished MPhil  
699 Thesis, School of Geography, University of Nottingham, UK, 205 pp.

700 Flood Action Plan-1 (FAP-1), 1991. River Training Studies of the Brahmaputra River,  
701 second interim report. Sir William Halcrow and Partners Ltd., London.

702 FAP-1, 1992. River Training Studies of the Brahmaputra River, draft final report. Sir  
703 William Halcrow and Partners Ltd., London.

704 Farge, M., 1992. Wavelet transforms and their application to turbulence. *Annual Review*  
705 *of Fluid Mechanics* 24, 395-457.

706 Ferguson, R.I., 1975. Meander irregularity and wavelength estimation. *Journal of*  
707 *Hydrology* 26, 315-333.

708 Ferguson, R.I., 1993. Understanding braiding processes in gravel-bed rivers: progress  
709 and unsolved problems. In: Best, J.L., Bristow, C.S. (Eds.), *Braided Rivers*. Geological  
710 Society Special Publication 75, Geological Society, London, pp. 73-87.

711 Fournier, A., 1995. Wavelets and their applications in computer graphics, SIGGRAPH'95  
712 Course Notes, pp. 5-35.

713 Fougere, P.F., 1985. On the accuracy of spectrum analysis of red noise processes using  
714 maximum entropy and periodogram methods: simulation studies and application to  
715 geophysical data. *Journal of Geophysical Research* 90(A5), 4355-4366.

716 Fraedrich, K., Jiang, J., Gerstengarbe, F-W., Werner, P.C., 1997. Multiscale detection of  
717 abrupt climate changes: application to the river Nile flood. *International Journal of*  
718 *Climatology* 17, 1301-1315.

719 Fu, S., Muralikrishnan, B., Raja, J., 2003. Engineering surface analysis with different  
720 wavelet bases. *Journal of Manufacturing Science and Engineering* 125, 844-852.

721 Gaucherel, C., 2002. Use of wavelet transform for temporal characterisation of remote  
722 watersheds. *Journal of Hydrology* 269, 101-121.

723 Gilbert, G.K., 1917. Hydraulic mining debris in the Sierra Nevada. US Geological Survey  
724 Professional Paper 105, pp. 1-154.

725 Goswami, D.C., 1995. Brahmaputra River, Assam, India: physiography, basin  
726 denudation and channel aggradation. *Water Resources Research* 21, 959-978.

727 Goswami, U., Sarma, J.N., Patgiri, A.D., 1999. River channel changes of the Subansiri in  
728 Assam, India. *Geomorphology* 30, 227-244.

729 Graps, A., 1995. An introduction to wavelets. *IEEE Computational Science and*  
730 *Engineering* 2, 50-61.

731 Grinsted, A., Moore, J.C., Jevrejeva, S., 2004. Application of the cross wavelet  
732 transform and wavelet coherence to geophysical time series. *Nonlinear Processes in*  
733 *Geophysics* 11, 561-566.

734 Gurley, K., Kareem, A., 1999. Applications of wavelet transforms in earthquake, wind,  
735 and ocean engineering. *Engineering Structures* 21, 149-167.

736 Gurnell, A.M., 1997. Channel change on the River Dee meanders, 1946-1992, from the  
737 analysis of air photographs. *Regulated Rivers Research and Management* 13, 13-26.

738 Gurnell, A.M., Downward, S.R., Jones, R., 1994. Channel planform change on the River  
739 Dee meanders, 1876-1992. *Regulated Rivers Research and Management* 7, 247-260.

740 Halcrow, Sir William and Partners, DHI, EPC and DIG, 1994. River Training Studies of the  
741 Brahmaputra River, Final Report, Annex 2: Morphology. Bangladesh Water Development  
742 Board (BWDB), Dhaka, Bangladesh. 88 pp.

743 Hooke, J., 1980. Magnitude and distribution of rates of river bank erosion. *Earth*  
744 *Surface Processes and Landforms* 5, 143-157.

745 Ikeda, S., Parker, G., Sawai, K., 1981. Bend theory of river meanders. part 1. linear  
746 development. *Journal of Fluid Mechanics* 112, 363-377.

747 ISPAN, 1995. The Dynamic Physical Environment of Riverine Charlands: Jamuna,  
748 Irrigation Support Project for Asia and near East (ISPAN), Flood Plan Coordination  
749 Organisation (FPCO), Dhaka, Bangladesh, 178 pp.

750 Johannesson, H., Parker, G., 1989. Linear theory of river meanders. In: Ikeda, H.,  
 751 Parker, G. (Eds.), River Meandering. Water Resources Monographs 12, American  
 752 Geophysical Union, Washington, DC. pp. 181-214.

753 Khan, N.I., Islam, A., 2003. Quantification of erosion processes in the Jamuna River  
 754 using geographical information systems and remote sensing techniques. Hydrological  
 755 Processes 17, 959-966.

756 Kleinhans, M.G., 2010. Sorting out river channel patterns. Progress in Physical  
 757 Geography 34, 287-326.

758 Kumar, P., Foufoula-Georgiou, E., 1997. Wavelet analysis for geophysical applications.  
 759 Reviews of Geophysics 35, 385-412.

760 Labat, D., 2005. Recent advances in wavelet analyses: Part 1. A review of concepts.  
 761 Journal of Hydrology 314, 275-288.

762 Labat, D., Ababou, R., Mangin, A., 1999. Wavelet analysis in karstic hydrology: part 1.  
 763 Comptes Rendues de l'Academie des Sciences: Geosciences de Surface 329, 881-887.

764 Labat, D., Ababou, R., Mangin, A., 2000. Rainfall-runoff relations for karstic springs.  
 765 Part II: continuous wavelet and discrete orthogonal multiresolution analyses. Journal of  
 766 Hydrology 238, 149-178.

767 Labat, D., Ababou, R., Mangin, A., 2002. Analyse multiresolution croisee de pluies et  
 768 debits de sources karstiques. Comptes Rendues de l'Academie des Sciences:  
 769 Geosciences de Surface 334, 551-556.

770 Lafreniere, M., Sharp, M., 2003. Wavelet analysis of inter-annual variability in the runoff  
 771 regimes of glacial and nival stream catchments, Bow Lake, Alberta. Hydrological  
 772 Processes 17, 1093-1118.

773 Lane, S.N., 2007. Assessment of rainfall-runoff models based upon wavelet analysis.  
 774 Hydrological Processes 21, 586-607.

775 Lane, S.N., Richards, K.S., 1997. Linking river channel form and process: Time space  
776 and causality revisited. *Earth Surface Processes and Landforms* 22, 249-260.

777 Latrubesse, E.M., 2008. Patterns of anabranching channels: the ultimate end-member  
778 adjustment of mega rivers. *Geomorphology* 101, 130-145.

779 Madej, M.A., Ozaki, V., 1996. Channel response to sediment wave propagation and  
780 movement, Redwood Creek, California, USE. *Earth Surface Processes and Landforms* 21,  
781 911-927.

782 Marcus, W.A., Fonstad, M.A., 2010. Remote sensing of rivers: the emergence of a  
783 subdiscipline in the river sciences. *Earth Surface Processes and Landforms* 35, 1867-  
784 1872.

785 Milne, A.E., Webster R., Lark, R.M., 2010. Spectral and wavelet analysis of Gilgai  
786 patterns from air photography. *Soil Research* 48, 309-325.

787 Mount, N.J., Louis, J., 2005. Estimation and propagation of error in measurements of  
788 river channel movement from aerial imagery. *Earth Surface Processes and Landforms*  
789 30, 635-643.

790 Mount, N.J., Louis, J., Teeuw, R.M., Zukowski, P.M., 2003. Estimation of error in  
791 bankfull width comparisons from temporally sequenced raw and corrected aerial  
792 photographs. *Geomorphology* 56, 65-77.

793 Nanson, G. C., Hickin, E.J., 1986. A statistical analysis of bank erosion and channel  
794 migration in western Canada. *Geological Society of America Bulletin* 97, 497-504.

795 Nason, G.P., 2008. *Wavelet Methods in Statistics with R*. Springer, New York. 260 pp.

796 Parker, G., Diplas, P., Akiyama, J., 1983. Meander bends of high amplitude. *Journal of*  
797 *the Hydraulics Division ASCE* 109, 1323-1337.

798 Percival, D.B., Wang, M., Overland, J.E., 2004. An introduction to wavelet analysis with  
799 applications to vegetation monitoring. *Community Ecology* 5, 19-30.

800 Phillips, J.D., 1999a. *Earth Surface Systems: Complexity, Order and Scale*. Blackwell,  
801 Oxford, 180 pp.

802 Phillips, J.D., 1999b. Methodology, scale and the field of dreams. *Annals of the*  
803 *Association of American Geographers* 89, 754-760.

804 Richardson, W.R., 1997. *Secondary Flow and Channel Change in Braided Rivers*.  
805 Unpublished PhD Thesis, School of Geography, University of Nottingham, UK, 281 pp.

806 Richardson, W.R., Thorne, C.R., 2001. Multiple thread flow and channel bifurcation in a  
807 braided river: Brahmaputra–Jamuna River, Bangladesh. *Geomorphology* 38, 185–196.

808 Rhoads, B.L., Thorn, C.R., 1996. *The Scientific Nature of Geomorphology*. Wiley,  
809 Chichester, 481 pp.

810 Sadowsky, J., 1996. Investigation of signal characteristics using the continuous wavelet  
811 transform. *Johns Hopkins APL Technical Digest* 17, 258-269.

812 Sankhua, R.N., Sharma, N., Garg, P.K., Pandey, A.D., 2005. Use of Remote Sensing and  
813 ANN in assessment of erosion activities in Majuli, the world's largest river island.  
814 *International Journal of Remotes Sensing* 26, 4445-4454.

815 Sarma, J.N., 2005. Fluvial processes and morphology of the Brahmaputra River in  
816 Assam, India. *Geomorphology* 70, 226-256.

817 Sarma, J.N., Basumallick, S., 1984. Bankline migration of the Burhi Dihing river, Assam.  
818 *Indian Journal of Earth Sciences* 11, 199-206.

819 Sarma, J.N., Phukan, M.K., 2004. Origin and some geomorphological changes of Majuli  
820 Island of the Brahmaputra River in Assam, India. *Geomorphology* 60, 1-19.

821 Sarma, J.N., Phukan, M.K., 2006. Bank erosion and bank line migration of the  
822 Brahmaputra river in Assam during the twentieth century. *Journal of the Geological*  
823 *Society of India* 68, 1023-1036.



824 Sarker, M.H., Thorne, C.J., 2006. Morphological response of the Brahmaputra-Padma-  
825 Lower Meghna river system to the Assam earthquake of 1950. In: Sambrook Smith, G.  
826 H., Best, J. L., Bristow, C.S., Petts, G. E. (Eds.), Braided Rivers: Process, Deposits,  
827 Ecology and Management. IAS Special Publication, 36, Blackwell Publishing, Oxford, pp.  
828 289-310.

829 Schumm, S.A., Lichty, E.W., 1965. Time, space and causality in geomorphology.  
830 American Journal of Science 263, 110-119.

831 Si, B.C., Farrell, R.E., 2004. Scale dependent relationships between wheat yield and  
832 topographic indices: A wavelet approach. Soil Science of America Journal 68, 577-588.

833 Singh, I.B., Bajpai, V.N., Kumar, A., Singh, M., 1990. Changes in the channel  
834 characteristics of Ganga River during late Pleistocene-Holocene. Journal of the  
835 Geological Society of India 36, 67-73.

836 Swanson, B.J., Meyer, G.A., Coonrod, J.E., 2011. Historical channel narrowing along the  
837 Rio Grande near Albuquerque, New Mexico in response to peak discharge reductions and  
838 engineering: magnitude and uncertainty of change from air photo measurements. Earth  
839 Surface Processes and Landforms 36, 885-900.

840 Takagi, T., Oguchi, T., Matsumoto, J., Grossman, M.J., Sarher, M.H., Matin, M.A., 2007.  
841 Channel braiding and stability of the Brahmaputra River, Bangladesh, since 1967: GIS  
842 and remote sensing analyses. Geomorphology 85, 294-305.

843 Thorne, C.R., Russell, P.G., 1993. Geomorphic study of bankline movement of the  
844 Brahmaputra River, Bangladesh. Proc. 5<sup>th</sup> Annual Seminar of the Scottish Hydraulics  
845 Study Group on Sediment Transport Processes and Phenomena. Edinburgh, UK.

846 Thorne, C.R., Russell, P.G., Alam, M.K., 1993. Planform pattern and channel evolution of  
847 the Brahmaputra River, Bangladesh. In: Best, J.L., Bristow, C.S. (Eds.), Braided Rivers.  
848 Geological Society of London Special Publication 75, Geological Society, London, pp. 257-  
849 276.

850 Thorne, C.R., Hossain, M.M., Russell, P.G., 1995. Geomorphic study of bank line  
851 movement of the Brahmaputra River in Bangladesh. *The Journal of the NOAMI* 12, 1-10.

852 Torrence, C., Campo, G.P., 1998. A practical guide to wavelet analysis. *Bulletin of the*  
853 *American Meteorological Society* 9, 61-78.

854 Torrence, C., Webster, P.J., 1999. Interdecadal changes in the ENSO-Monsoon system.  
855 *Journal of Climate* 12, 2679-2690.

856 Van Gerven, L.P.A., Hoitink, A.J.F., 2009. A new method to analyze the geometry of a  
857 river: wavelet analysis on the curvature series. Application to the Mahakam River  
858 indicates geometric zoning. In: Vionnet, C.A., García, M.H., Latrubesse, E.M., Perillo,  
859 G.M.E. (Eds.) 6th IAHR Symposium on River, Coastal and Estuarine Morphodynamics,  
860 Santa Fe, Argentina, 21 to 25 September 2009, 7 pp.

861 Wathen, S.J., Hoey, T.B., 1998. Morphological controls on the downstream passage of a  
862 sediment wave in a gravel-bed stream. *Earth Surface Processes and Landforms* 23,  
863 715-730.

864 Zolezzi, G., Seminara, G., 2001. Downstream and upstream influence in river  
865 meandering. Part 1. General theory and application to over-deepening. *Journal of Fluid*  
866 *Mechanics* 438, 183-21.

867

868 **Table 1.** Images used to derive the bank line migration series.

Image Date	Sensor	Resolution	Acquisition Date	Q at Bahadurabad (m <sup>3</sup> sec <sup>-1</sup> )
1987	Landsat MSS	80m x 80m	7 Feb	4000
1989	Landsat TM	30m x 30m	28 Feb	6070
1992	Landsat TM	30m x 30m	8 Mar	4660
1994	Landsat TM	30m x 30m	25 Jan	5070
1995	Landsat TM	30m x 30m	28 Jan	4550
1996	Landsat TM	30m x 30m	31 Jan	4680
1997	Landsat TM	30m x 30m	18 Feb	No Data
1998	Landsat TM	30m x 30m	5 Feb	3710
1999	Landsat TM	30m x 30m	23 Jan	4830

869

870

871 **Table 2.** Characteristic reach types at the 0-10 km scale band.

<b>Downstream Distance</b>	<b>Reach Character</b>	<b>Description</b>
0 - 8 km	COI	Falls within the COI.
8 - 57 km	Transient and Variable Magnitude	Reach contains significant wavelet power of low, moderate and high magnitudes, but which is temporally and spatially transient. Bank retreat is evident at scales of 0-10 km, but its location and magnitude exhibits a high degree of temporal variability. There is strong evidence of downstream migration of bank line retreat.
57 - 65 km	Low Magnitude	Little or no significant wavelet power at any time period. There is little evidence of bank retreat operating at scales between 0-10 km.
65 - 85 km	Persistent and High Magnitude	Reach has a consistent spatial and temporal pattern of significant wavelet power of medium and high magnitude. Substantive bank retreat at scales of 0-10 km is occurring throughout the study period.
85 - 120 km	Transient and Moderate Magnitude	Reach contains significant wavelet power of low and moderate magnitudes and which is temporally and spatially transient. Moderate bank retreat is occurring at scales of 0-10 km. There is evidence of downstream migration of bank line retreat.
120 - 135 km	Low Magnitude	Little or no significant wavelet power at any time period. There is little evidence of bank retreat operating at scales between 0-10 km.
135 - 155 km	Persistent and High Magnitude	Reach has a consistent spatial and temporal pattern of significant wavelet power of moderate and high magnitudes. Substantive bank retreat at scales of 0-10 km is occurring throughout the study period.
155 - 164 km	Low Magnitude	Little or no significant wavelet power at any time period. There is little evidence of bank retreat operating at scales between 0-10 km. This stable reach is probably a result of the guide bunds of the Jamuna Bridge.
164 - 196 km	Transient and Variable Magnitude	Reach contains significant wavelet power of low, moderate and high magnitudes, but it is temporally and spatially transient. Bank retreat is occurring at scales of 0-10 km, but its location and magnitude exhibit a high degree of temporal variability. There is strong evidence of downstream migration of bank line retreat.
COI 196 - 204 km	COI	Falls within the COI.

872

873

874 **Table 3.** Maximum daily mean discharge (QMax) and the number of days exceeding the  
875 total study period 95<sup>th</sup> percentile discharge (Q<sup>95</sup>) for each time period.

Time Period	QMax recorded at Bahadurabad (m <sup>3</sup> sec <sup>-1</sup> )	Days exceeding Q <sub>95</sub>
1987-89	98,300	42
1989-92	84,100	60
1992-94	67,000	18
1994-95	40,900	0
1995-96	87,000	15
1996-97	83,800	21
1997-98	79,219	5
1998-99	103,128	48

876

877

878

**Figure 1.** Mother wavelets for A. Morlet ( $k=6$ ), B. Morlet ( $k=3$ ), C. Paul ( $k=3$ ) and D. DOG ( $k=3$ ).

**Figure 2.** The location of the study reach showing the confluence with the Teesta River (A), the location of the Bahadurabad gauging station (B), the approximate position of the guide bunds of the Jamuna Bridge (C) and the confluence with the Ganges River (D). Note that the main channel is orientated due north-south.

**Figure 3.** The temporal sequence of 1987-1999 bank line retreat series for the Jamuna river LHB.

**Figure 4.** CWT for 1998-99 bank line retreat series using Morlet  $k = 3$  and  $k = 6$ , Paul  $k = 3$  and DoG  $k = 3$  mother wavelets. The bold line shows the 95% confidence level (i.e. regions within the line have significant wave power over a background red noise spectrum  $\alpha = 0.72$ ). The thin dashed line shows the COI. Regions within the COI should be interpreted with caution.

**Figure 5.** CWT power spectra (Morlet  $k=3$  wavelet function) for bank line retreat series for all time periods. The bold line shows the 95% confidence level (i.e. regions within the line have significant wave power over a background red noise spectrum). The thin line indicates the COI. Regions within the COI should be interpreted with caution.

**Figure 6.** Scale averaged wavelet power spectra for 0-10 km and 10-30 km scale bands. Data are plotted as multiples of the wavelet power value equal to the 95% confidence level. The analysis ignores the regions of the plots where variation of wavelet power occurs within the cone of influence (labelled COI).

**Figure 7.** Daily mean discharge at Bahadurabad for the 1987-1999 study period. The portion of the hydrograph within each time period is indicated.

**Figure 8.** The relationship between  $Q_{\text{Max}}$  and the integral of the scale-averaged wavelet power spectrum for scale bands 0-10 km, 10-20 km, 20-30 km, 30-40 km and 40-50 km.

**Figure 9.** The relationship between the number of days for which flow exceeds the 95<sup>th</sup> percentile for the study period ( $Q_{95}$ ) and the integral of the scale-averaged wavelet power spectrum for scale bands 0-10 km, 10-20 km, 20-30 km, 30-40 km and 40-50 km.

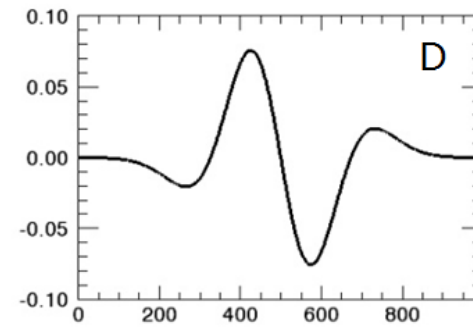
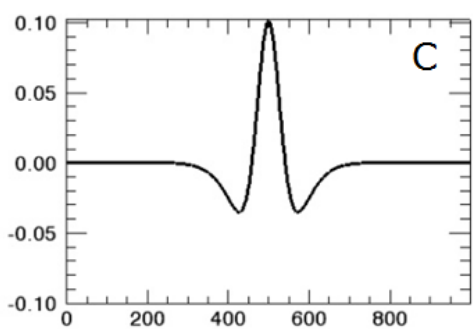
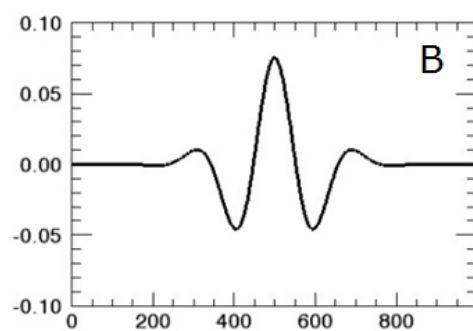
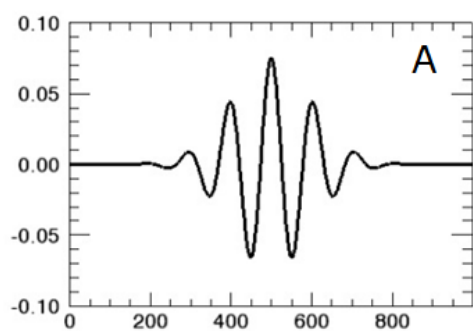


**Figure 1**

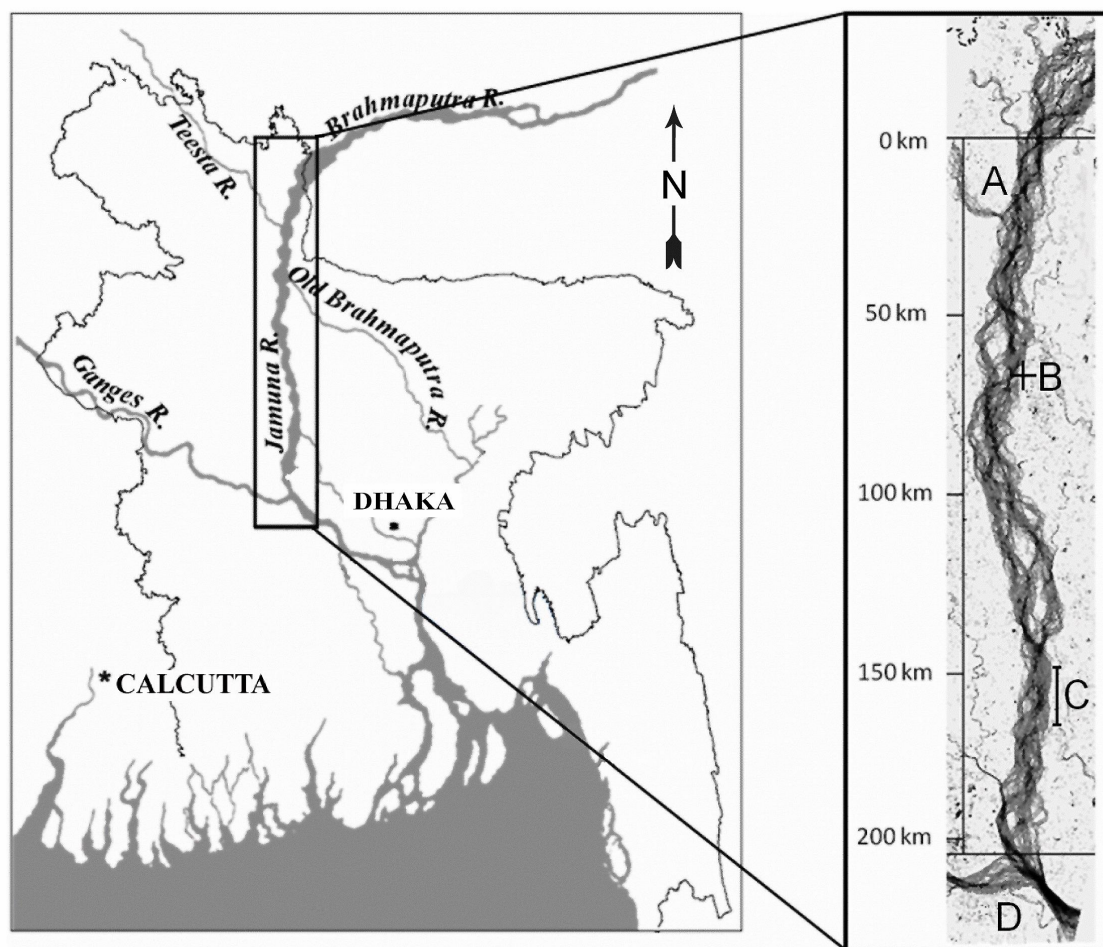
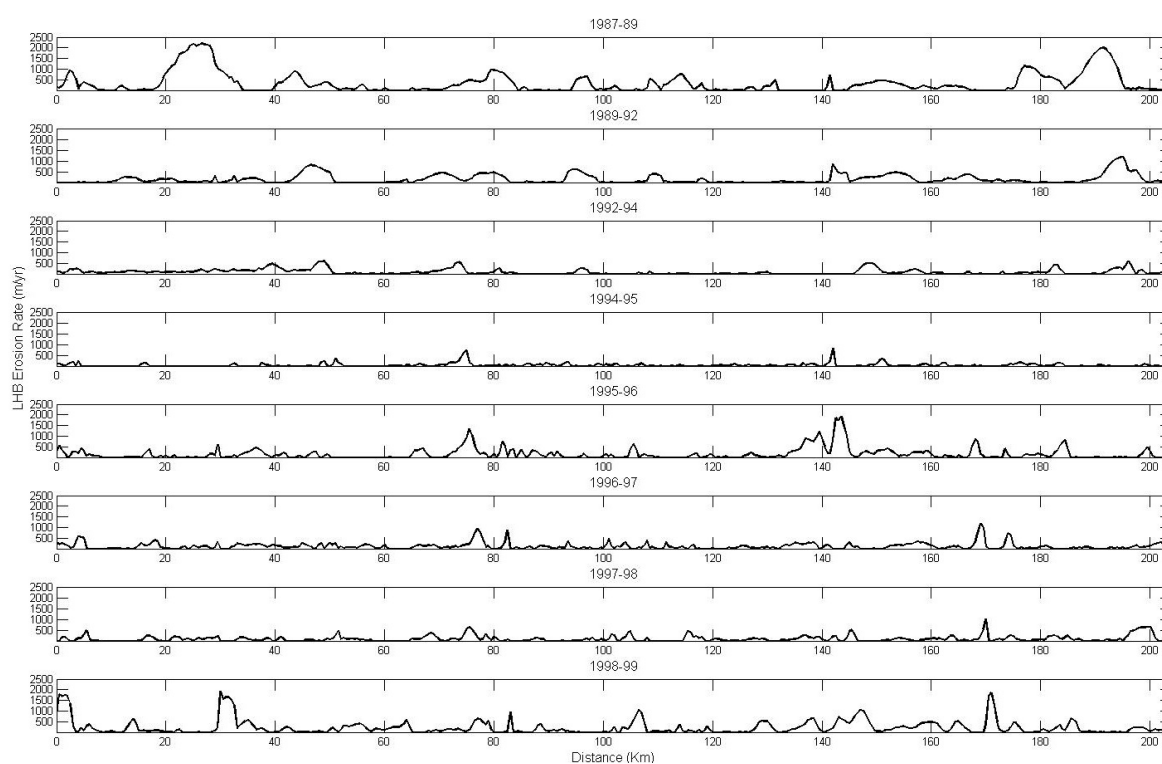
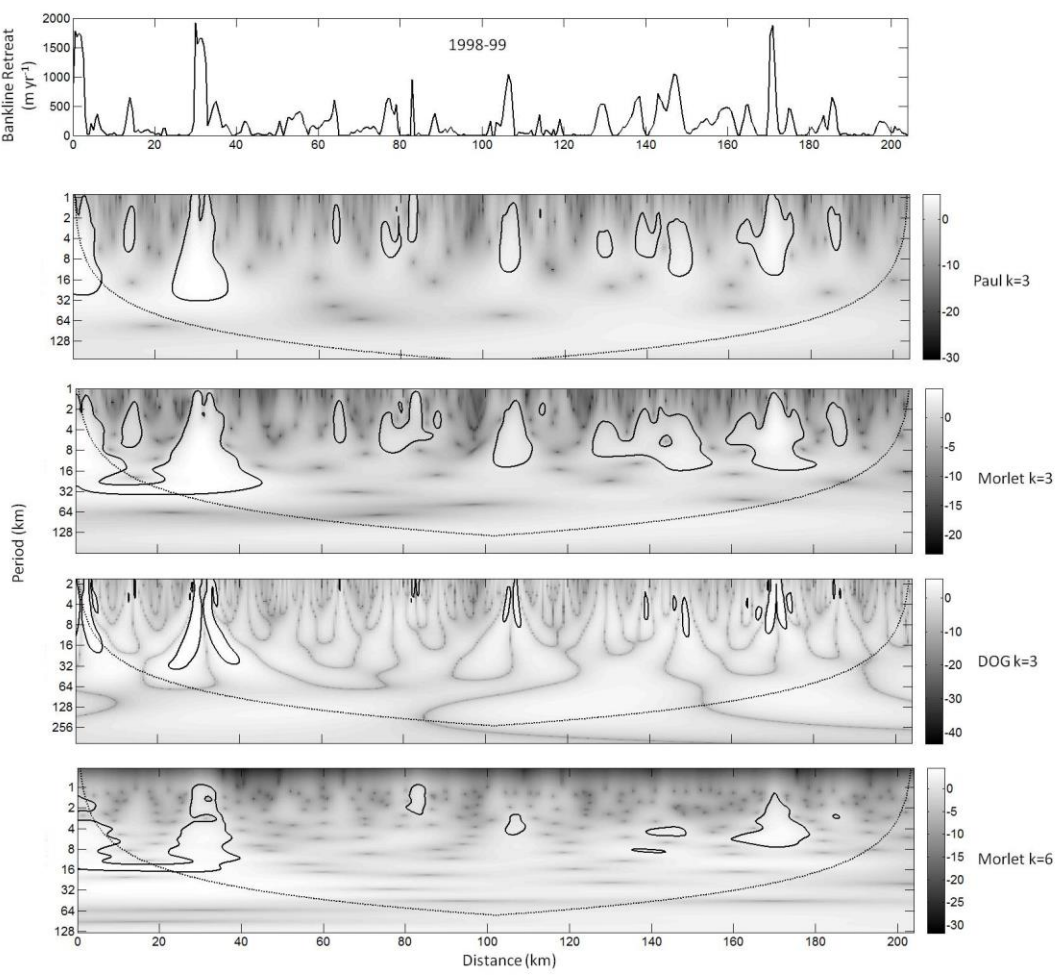


**Figure 2**

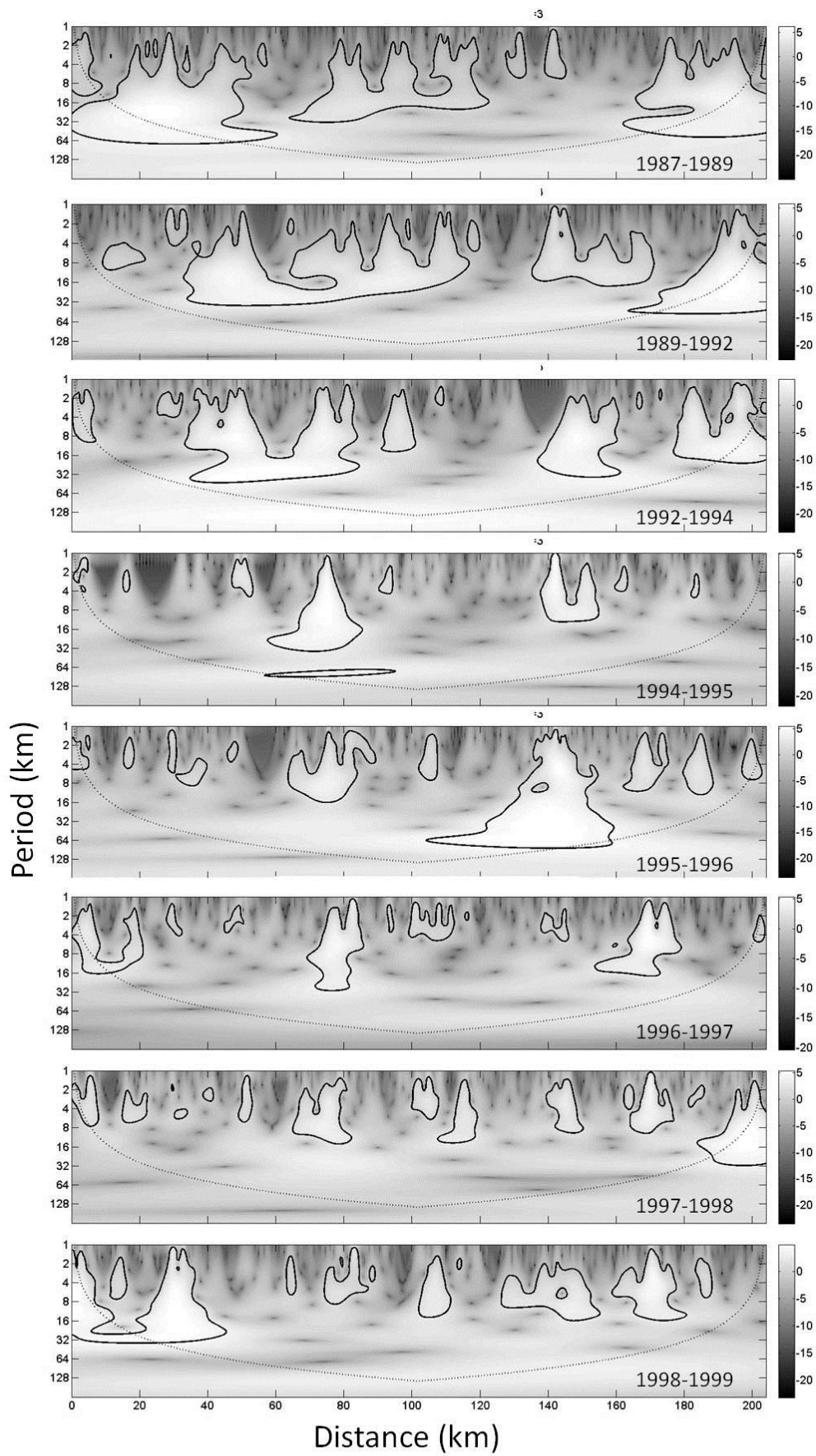




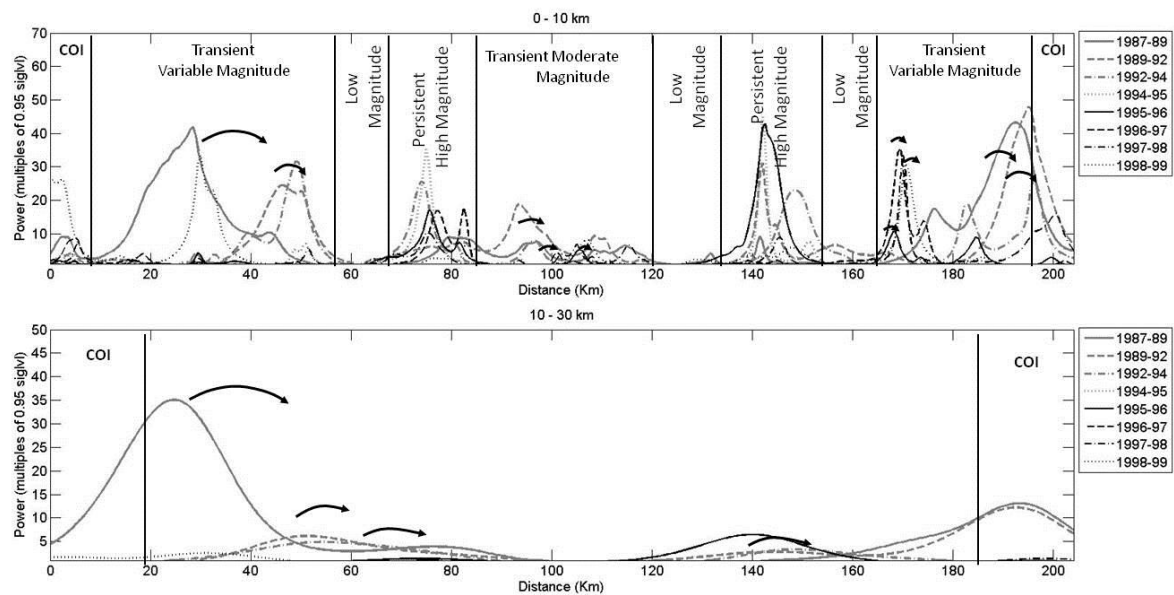
917 **Figure 3**  
918



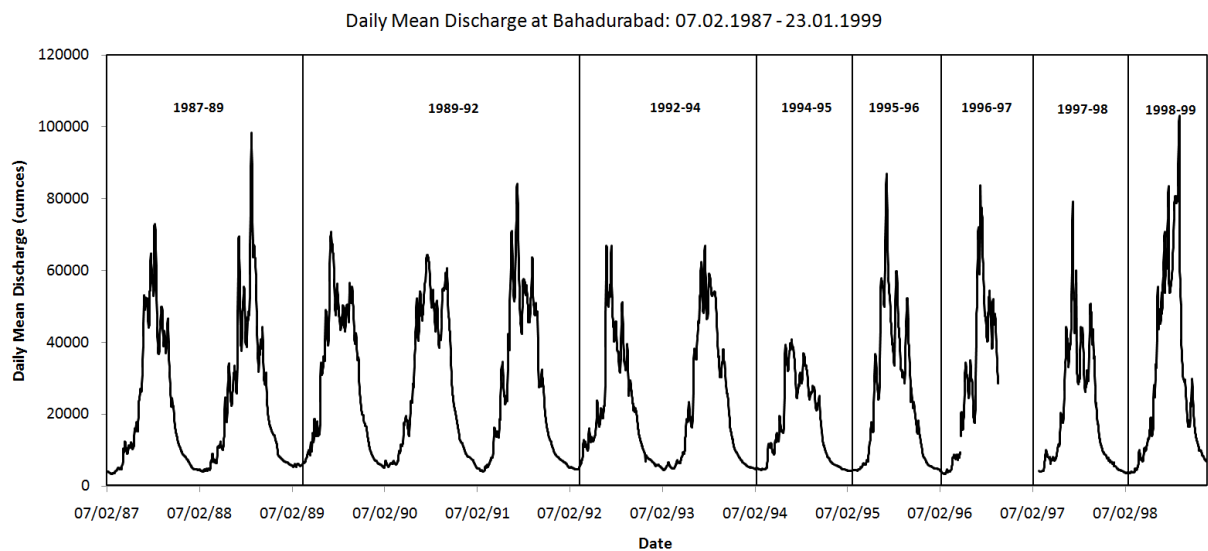
919 **Figure 4**  
920  
921



923 **Figure 5**  
924



925 **Figure 6**  
926  
927



928 **Figure 7**  
929  
930

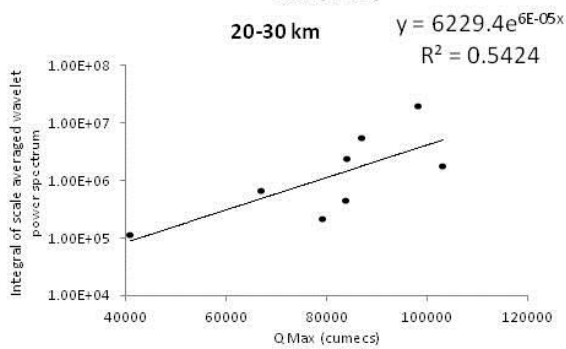
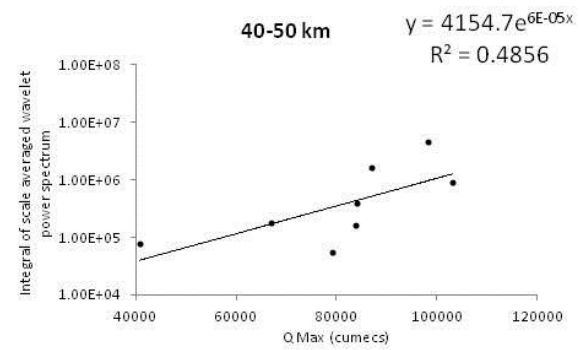
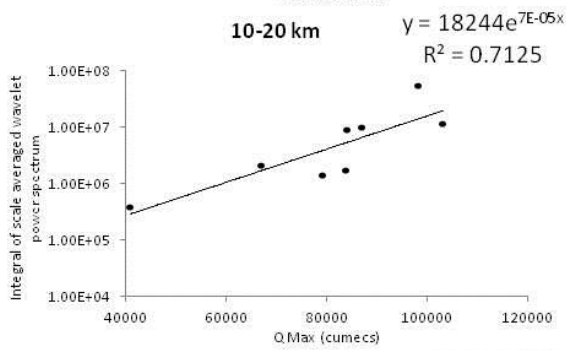
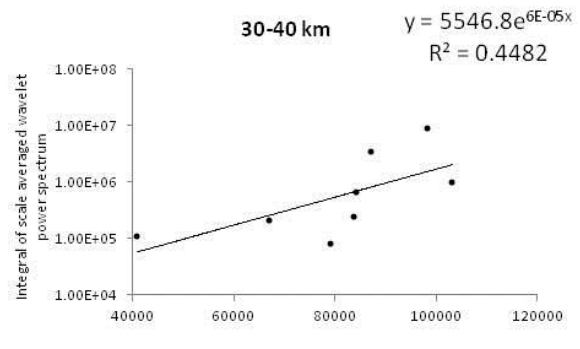
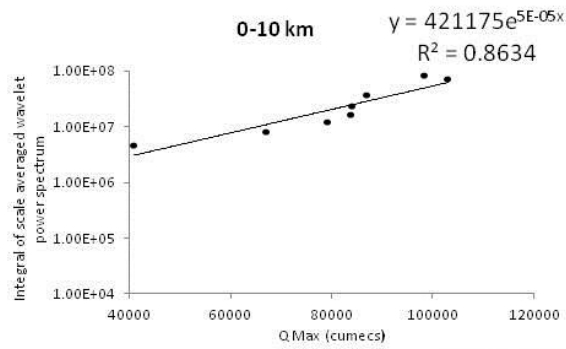


**Figure 8**

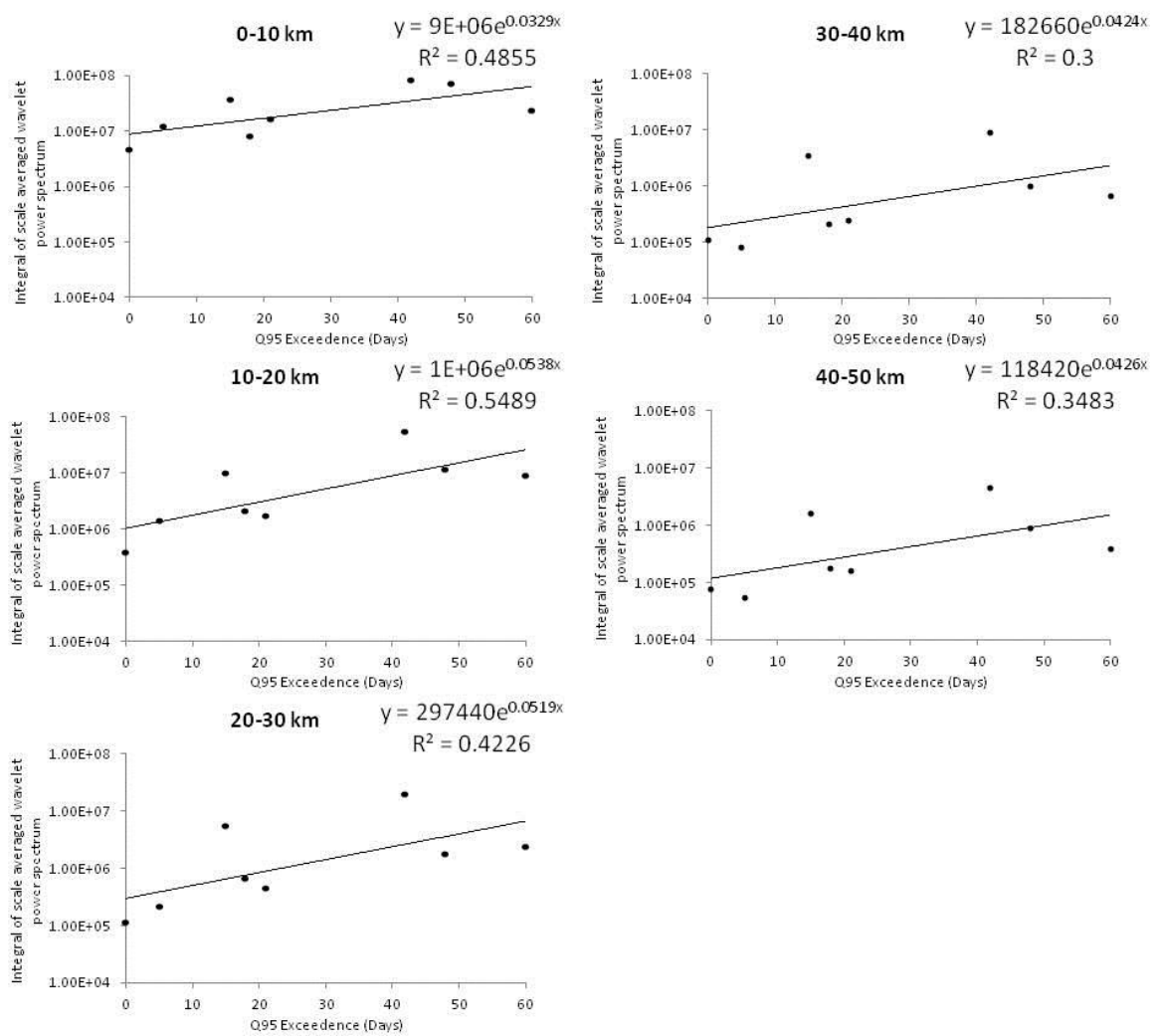


**Figure 9**